UCSF

UC San Francisco Electronic Theses and Dissertations

Title

Analysis of Craniofacial and Dental Abnormalities in a novel mouse model for Alagille Syndrome

Permalink

https://escholarship.org/uc/item/1tx371zh

Author

Tahk, Ji Hyun (Caroline)

Publication Date

2021

Peer reviewed|Thesis/dissertation

Analysis of Craniofacial and Dental Abnormalities in a novel mouse model for Alagille Syndrome
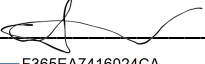
by
Ji Hyun Tahk

THESIS
Submitted in partial satisfaction of the requirements for degree of
MASTER OF SCIENCE

in
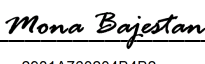
Oral and Craniofacial Sciences

in the

GRADUATE DIVISION
of the
UNIVERSITY OF CALIFORNIA, SAN FRANCISCO

Approved:

DocuSigned by:

_____   Andrew Jheon
F365EA7416024CA...
                                                                                                    Chair

DocuSigned by:

_____   Nathan Young
Nathan Young

DocuSigned by:

_____   Mona Bajestan
Mona Bajestan
2981A760204B4B2...

_____

_____
                                                                                      Committee Members

Analysis of Craniofacial and Dental Abnormalities in a novel mouse model

for Alagille Syndrome

Ji Hyun Tahk

<u>**Abstract**</u>

Alagille Syndrome is a multisystem genetic disorder characterized by chronic cholestasis, cardiovascular anomalies, ocular abnormalities, skeletal defects, and characteristic facial features. Mutations in Jagged1 (Jag1), a key ligand in the Notch signaling pathway, are associated with the majority of cases. The Notch signaling pathway plays important roles in the development and homeostasis of most, if not all tissues. However, the roles of Jag1 and the Notch signaling pathway in craniofacial and dental development remain unclear. This study aimed to elucidate the roles of Notch signaling pathway in craniofacial and dental development using a mouse model of Alagille Syndrome ($Jag1^{Ndr/Ndr}$ mice, which possess a missense mutation (H268Q) in $Jag1$). Embryonic and postnatal mouse specimens were collected at various stages from $Jag1^{Ndr/Ndr}$ mice. Micro-computed tomography (microCT) and three-dimensional (3D) Geometric Morphometric Analysis (GMA) were performed on adult skulls to analyze changes in craniofacial morphology. Hematoxylin and eosin (H&E) staining on histological sections was performed on control and $Jag1^{Ndr/Ndr}$ mice at embryonic day (E)14.5, E16.5, postnatal (P)0, and P7 to analyze tooth development. 3D GMA showed variations in the coronoid process, zygomatic process, and the area where parietal, occipital, and squamosal bones intersect in $Jag1^{Ndr/Ndr}$ mutant mice. In addition, mutants had more convex crania from both frontal and lateral views and a longer snout. Our histological analysis of tooth development showed defects in cell-matrix adhesion (ameloblast-enamel matrix) and cell-cell adhesion (ameloblast-stratum intermedium) at

P7. MicroCT analysis of P7 and adult molars supported our histological findings and revealed changes in tooth morphology. Disruption in Notch signaling due to a missense mutation (H268Q) in *Jag1* led to: 1) specific changes in craniofacial morphology; 2) defective cell-matrix and cell-cell attachments during tooth development; 3) possible changes in tooth structures due to abnormal tooth development and mineralization. Our study demonstrates for the first time that Notch signaling is essential for specific changes in craniofacial morphology and proper dental development.

Table of Contents

List of Figures

List of Tables

1. Introduction

1.1 Alagille syndrome

Alagille Syndrome is a rare, complex, multisystem disorder first reported by Alagille *et al.* in 1975 (1). ALGS is an autosomal dominant genetic disorder with an incidence of approximately 1 in 70,000 to 100,000 live births. Traditionally, the diagnosis of ALGS has been based on histological findings of bile duct paucity, in addition to three or more of the following five major features: chronic cholestasis, cardiovascular anomalies, ocular abnormalities, skeletal defects, and characteristic facial features (2). The clinical diagnosis of ALGS is characterized by a reduced number of bile ducts within the liver, but is distinguished from other liver disorders because of combined abnormalities in other structures, such as heart, eyes, face, and skeleton (3). Abnormalities in other organs include renal defects, pancreatic insufficiency, hypothyroidism, and delayed puberty.

The severity and clinical significance of ALGS phenotype are highly variable (2). The mortality rate is approximately 10% with vascular accidents, cardiac disease, and liver disease being responsible for most of the deaths (4). However, ALGS with severe liver or cardiac involvement is most often diagnosed in infancy, and 25% of patients tend to die before the age of five because of the cardiovascular and hepatic complications. ALGS with subclinical or mild hepatic manifestations may not be established until later in life and this presentation is usually benign.

Hepatic manifestations can range from mild cholestasis and pruritus to progressive liver failure (3). The majority of symptomatic patients have jaundice, and chronic cholestasis occurs in a very high proportion of patients. Liver function test results show increased serum bile acids, conjugated bilirubin, alkaline phosphatase, cholesterol, and

gamma-glutamyltranspeptidase. Such laboratory results indicate defects in biliary excretion. Liver biopsy of approximately 15% of ALGS cases show progressive liver disease, leading to cirrhosis and liver failure requiring transplantation. However, there is currently no reliable method to predict whether patients will progress to end-stage liver disease and require transplantation (5).

More than 90% of ALGS patients also present with cardiac disease, most commonly involving pulmonary valve, artery, and branches with peripheral pulmonary stenosis (2). Tetralogy of Fallot is the most reported cardiac malformation associated with ALGS (3). Other cardiovascular involvements include ventricular septal defect, atrial septal defect, aortic stenosis, coarctation of the aorta, pulmonary atresia, and hypoplastic left heart syndrome.

The most common eye involvement in 90% of ALGS patients is posterior ocular embryotoxon (3). Posterior embryotoxon is a corneal abnormality with a thin grey-white, arcuate ridge on the inner surface of the cornea, adjacent to the limbus. There are various ophthalmic features involved with the cornea, iris, retina, and optic disc. In the majority of ALGS patients, however, visual acuity may not be affected, although a small decrease in acuity may occur.

Skeletal abnormalities in ALGS have been well-documented since 1980 (6). Butterfly vertebrae are the most common skeletal anomalies seen in approximately 50% of ALGS patients (2). It is due to the failure of the anterior vertebral arches to fuse but is asymptomatic in most patients (3). Other bony manifestations in patients with ALGS have been described less frequently (7).

The presence of craniofacial abnormalities are often essential clinical findings that are significant in diagnosing ALGS. Alagille et al. reported that the facial phenotype was present in 95% of 80 reviewed cases (8). Later studies by Emerick et al. found a similar frequency of 96% in a series of 92 patients (2). Notable craniofacial dysmorphisms related to ALGS include craniosynostosis, prominent forehead, moderate hypertelorism with deep-set eyes, a saddle or straight nose with a flattened, bulbous tip, and large ears (9). These features are less noticeable before the age of 1, but a prominent forehead and a delicate pointed chin develop later in life (3). Around puberty, the chin becomes more prominent, leading to a more prognathic profile, but the forehead prominence becomes less dominant.

Although not as prevalent as other ALGS facial phenotypes, craniosynostosis has also been reported as another craniofacial anomaly associated with ALGS. Kamath et al. gave the first description of craniosynostosis in ALGS with unilateral left coronal synostosis found in two ALGS patients (9). Craniosynostosis is a premature fusion of cranial sutures and may present with only one suture fused or two or more sutures fused. It may also be defined as either isolated or syndromic, depending on whether other primary defects are present. Isolated craniosynostosis has no other abnormalities other than early sutural fusion, whereas syndromic craniosynostosis has other underlying morphogenic abnormalities present. Syndromic craniosynostosis has been well-documented at the molecular level, particularly mutations involving fibroblast growth factor receptor 1, 2, and 3 (FGFR1, -2, and -3) genes (9). Many studies have alluded to the clinical overlap between the FGF and Notch pathways, which has been known to play a contributory role in the development of ALGS. A mouse study involving the neuroepithelial precursor cells suggests that the inhibitory action of FGF1 and FGF2 is controlled by the Notch pathway (9,10).

Another mouse dental epithelium study indicates that the FGF signaling regulates the Notch pathway in determining the fate of stem cells (9,11).

Depending on the severity of the disease, ALGS may also affect dentition, salivary glands, periodontium, and mucous membranes (3). To date, oral findings have not been a primary concern in ALGS, but both the primary and permanent dentition maybe heavily affected possibly due to complications of cholestasis and hyperbilirubinemia. As a result, enamel opacities, hypomineralization, and enamel hypoplasia have been reported (12). Higher serum bilirubin levels more than 30 mg/dl during development may also lead to significant changes in dental tissues (13). Several studies have reported abnormal pigmentation related to ALGS as bilirubin accumulates during tooth development and causes variable, greenish-brown discoloration (13–16).

In addition to the effects on the color and mineralization, ALGS may be also associated with deformed tooth morphology and reduced number of teeth. There has been a limited number of reports on the presence of talon cusps in primary and permanent dentition, as well as macrodontic maxillary incisors and taurondontic deciduous teeth with a widened pulpal cavity linked to ALGS (17,18). Other studies have suggested hypodontia and tooth agenesis related to ALGS (12,19). These abnormal tooth shape and number may lead to clinical concerns regarding compromised esthetics, malocclusions, increased caries risk, and patient discomfort. The presence of macrodontic incisors or an accessory cusp, especially on anterior teeth, will not only cause a patient's esthetic concerns, but also occlusal disharmony. The discrepancies related tooth size and form may lead to occlusal interferences and increase the risk of tooth fracture. While the extra cusp usually blends

smoothly with the tooth, the pronounced groove on the talon cusp easily retains plaque, making the tooth more susceptible to caries.

The diagnosis of ALGS is based on clinical criteria as well as genetic testing involving Jagged1 (Jag1) and Notch genes. According to genetic testing, 94-96% of ALGS cases are caused by Jag1 mutations (ALGS1) and around 1% by Notch2 mutations (ALGS2) (4). Jag1 is a ligand in the Notch signaling pathway that determines cell fate early in life and the Notch receptors are transmembrane proteins that interact with their ligands to trigger a cascade of intracellular downstream effects, leading to cell fate determination and differentiation (9,20). The Notch receptor on a signal-receiving cell activates the Jag1 ligand on a signal-sending cell upon direct contact. A deletion or mutation of a single copy of Jag1 on chromosome 20p12 has been documented to be the cause of genetic defect in the majority of ALGS patients (16). The pathogenic mechanism behind Jag1 mutation causing ALGS suggests that Jag1 mutations mostly lead to protein-truncating variants (75%), including frameshift, non-sense, exon level deletion, and splice site (21,22). Jag1 homozygous knockout mice showed early lethality from vascular defects (23), whereas Jag1 heterozygous knockout mice revealed ocular abnormalities alone (24). Compound heterozygous mice with Jag1 and Notch2 mutations presented with certain phenotypes of ALGS, including hepatic, cardiac, ocular, and renal conditions (24). ALGS patients with Notch2 mutations show frequent cardiac anomalies and milder renal problems compared to the Jag1 variants (20,25).

Compared to the extensive studies on Jag1 mutations related to ALGS, the pathogenic mechanism of Notch2 mutations is not clearly understood. It is possible that ALGS patients with Notch2 mutations are less frequently identified, and therefore, pose

challenges in studying these variants. Some studies have suggested, however, that Notch2 variants are predominantly missense mutations in ALGS patients (26,27). Far fewer cases with Notch2 mutations compared to Jag1 mutations in ALGS patients may suggest that missense mutations in Notch2 are less tolerated, and patients with these variants are more likely to suffer functional consequences. Nevertheless, the findings that Jag1 mutations can lead to ALGS suggest that Notch signaling is essential in the normal development of the liver, heart, skeleton, eyes, face, and kidney. (5).

1.2 Tooth development

Notch signaling in ALGS has shown to play significant roles not only in skeletal and craniofacial systems, but also in tooth development. Tooth development involves sequential interactions between neighboring epithelial and mesenchymal cells (28). Previous literature has suggested cell fate determination and differentiation of various cell types in distinct tooth development stages. Teeth arise from continuous interactions between cranial neural crest-derived mesenchymal cells and oral ectoderm (29). The mesenchymal cells that lie directly under the epithelium differentiate into odontoblasts that secrete the dentin organic matrix. These mesenchymal cells also come into close contact with epithelial cells and differentiate into ameloblasts that generate the enamel matrix (29).

This process called amelogenesis, or enamel formation, is the mechanism by which ameloblast cells differentiate and secrete enamel matrix, which eventually mineralizes to form enamel. The epithelial-derived enamel organ (EO) gives rise to the inner enamel epithelium (IEE), which differentiates into enamel-forming ameloblasts (30). During this

process of differentiation and maturation, the basal surface of ameloblasts is attached to the stratum intermedium (SI) (31). The SI and stellate reticulum (SR) layers combine to form the papillary layer at the transitional and mature stages. As the tooth erupts in the final stages, SI, SR, outer enamel epithelium (OEE), and ameloblasts are sloughed off, leaving the uncovered enamel with neither cells nor organic matrix (30).

1.3 Notch signaling pathways

The process of tooth development involves tight regulation of Bmp, Fgf, Shh, and Wnt signaling pathways (32). Several studies have also suggested the importance of Notch signaling in tooth development, but relatively little is known about the roles of Notch signaling during amelogenesis. Notch signaling is a major pathway important in cell-cell interactions. The role of Notch signaling is especially crucial during development where signal transmitted through the Notch surface receptor determines the fate of one cell with its neighboring cells through physical interactions between the Notch receptor and the membrane-bound ligands (33). It is a highly conserved cell-contact dependent signaling pathway and encodes 5 receptors (Notch 1-5) (34). Components of the Notch signaling pathway in mammals include 4 transmembrane Notch receptors (Notch1-4) and 5 ligands (Jag1, Jag2, Dll1, Dll3, and Dll4). Mutations in the Notch pathway led to numerous diseases, including ALGS (33). This pathway functions in an enormous diversity of developmental processes and its dysfunction is implicated in many cancers.

The structure of Notch receptors varies by type, but they include an extracellular domain (NECD), a negative regulatory region (NRR), and an intracellular domain (NICD) (34). Notch receptors interact with membrane-bound ligands and are activated through the

release of the Notch intracellular domain (NICD). NICD translocates to the nucleus where it forms a transcriptional activator complex with the DNA-binding protein CSL (CBF1/RBP-J in mammals, Suppressor of Hairless [Su(H)] in Drosophila and Xenopus and Lag-1 in Caenorhabditis elegans) along with transcriptional co-activators to activate Notch target genes (33). CSL has been well characterized and is considered to be the primary target of Notch signaling in mammalian cells that represses and activates transcription in the absence and presence of Notch signaling, respectively. The NICD-CSL complex activates transcription through recruitment of the histone acetyltransferase PCAF.

Previous study on the effects of Notch signaling inhibition in mouse tooth development has suggested that Notch signaling is not only important in enamel mineralization, but also crucial in cell-cell adhesion and the ameloblast-SI interface (32). Normal enamel is composed of mineralized rods that extend from the dentin-enamel junction (DEJ) to the enamel surface. These highly organized enamel rods run parallel in the same direction from the DEJ to the enamel surface. Jheon et al. found that the microarchitecture of the enamel rods appeared to be smaller and rounder in Notch inhibition models. Furthermore, Notch signaling seemed to play critical roles in ameloblast-SI and SI-SI adhesion, partly due to changes on specific components of desmosomes. It has been implicated that the expression of Notch genes was seen in cells located in SI (29). When Notch signaling was inhibited, it was clear that the inhibition led to ameloblast-ameloblast detachment, proven by the increased spaces between ameloblasts. These spaces were often filled with what appeared to be either cellular debris or cell processes (32). Desmosomes, which are transmembrane complexes that provide strong cell-cell adhesion, appeared to be mutated with Notch signaling inhibition.

Notch signaling also plays an important role in regulating chondrogenesis and osteoblastogenesis during skeletal development (34). Chondrogenesis is a process by which cartilage is formed from condensed mesenchymal tissue, leading to bone formation via endochondral ossification. Notch signaling inhibition during chondrocyte differentiation increases chondrocyte proliferation, and eventually results in decreased bone formation (35). During osteoblastogenesis, osteoblast precursor cells proliferate and differentiate (34). Similar to its role in chondrogenesis, Notch signaling plays an inhibitory function in the later stages of osteoblastogenesis by downregulating transcription factors, such as Runx2, involved in the process (36). Notch signaling affects bone mineralization during skeletal development, and abnormal Notch signaling has been suggested in several genetic and sporadic disorders that influence the skeletal system, including the craniofacial area.

1.4 Geometric Morphometrics

On a larger scale, changes in macrostructures due to Notch signaling can be studied using geometric morphometrics (GMA). Morphometrics is a valuable tool that can measure and characterize organismal forms to quantify morphological variations. Traditionally, it has been used to describe diversity among different species and organisms in the fields of systematics, evolutionary biology, and physical anthropology. The use of GMA has recently been extended to assess morphological abnormalities in developmental biology, ecology, and different medical disciplines as well.

Variations across complex craniofacial structures are difficult to capture with two-dimensional (2D) analysis. However, the limitations of 2D analysis in measuring linear and

angular measurements as well as shape and size can be overcome by using micro-computed tomography (microCT) with three-dimensional (3D) GMA (37, 38). 3D GMA places specific landmarks on essential parts of the structures to be analyzed, and thereby, evaluates 3D shape variation between specimens in a non-biased manner (39). Despite its advantages over 2D analysis, the landmark-based 3D GMA has its own drawbacks in that characterizing organismal forms and 3D shapes with more complex structures, such as the condyle and glenoid fossa, are more difficult to accurately quantify with insufficient landmarks to represent 3D shape (40).

To overcome such challenges, semi-/pseudo-landmarks were introduced as a supplementary method to define more complex 3D shapes (41). The semi-/pseudo-landmarks helped to improve characterizing complicated shapes by densely placing distinct points on the homologous structure across specimens, not within or between them (40). These sets of points can be used to establish complex shapes in different samples to represent homologous curves and surfaces on a 3D level.

2. Central Hypothesis

We hypothesize that there will be specific changes in craniofacial and dental morphology and development associated with alterations in Notch signaling in $Jag1^{Ndr/Ndr}$ mice, a model for ALGS1.

3. Specific Aims

Our first aim is to determine the effects of Notch signaling on craniofacial morphology using 3D GMA in $Jag1^{Ndr/Ndr}$ mice. Our second aim is to determine the role of Notch signaling on tooth development, using histological and microCT analyses.

4. Materials and Methods

4.1 Animals and specimen numbers

Mice with a missense mutation (H268Q) in *Jag1* (*Jag1*$^{Ndr/+}$ mice) were outbred to a

C3H/C57bl6 background. Male and female *Jag1*$^{Ndr/+}$ mice were mated to generate control

(*Jag1*$^{+/+}$ and *Jag1*$^{Ndr/+}$) and mutant (*Jag1*$^{Ndr/Ndr}$) mice, hereafter also referred to as Ndr

mutants (25). Collected specimens were fixed in 4% paraformaldehyde and sent to us from

our collaborator (Emma Andersson, Karolinska Institutet, Sweden). Adult control (n=4)

and mutant (n=4) male mice at 7-8 months of age were analyzed using 3D GMA. Control

and Ndr mutant mice at E14.5 (n=3), E16.5 (n=3), P0 (n=3), and P7 (n=3) were analyzed by

histology.

4.2 Image processing and landmark data collection protocol

Fixed mouse heads were subjected to microCT using a SkyScan 1076 MicroCT at the

Small Animal Tomographic Analysis Facility (SANTA) located at Seattle Children's Research

Institute. Specimens were scanned at 17.2-micron resolution (55 kV, 150 mA, 0.5 mm Al

filter). Reconstructions were generated using NRecon (Version 1.6.9.4) with consistent

thresholding parameters, and then converted to 3D volumes. Skull segmentations from

microCT data were performed with Avizo Lite (version 9.1.1).

Geometric morphometric analysis (GMA)

Three-dimensional (3D) coordinate locations of 44 landmarks on the skull and 13

landmarks on the mandible of controls (N= 4 males) and mutants (N= 4 males) of 7-8

months of age were marked using Landmark software (Fig.1) (42). The observer was

blinded to each mouse during data collection. To determine the accuracy and reproducibility of landmark identification, an initial random subset of 2 samples was landmarked twice using the 44 skull (cranium including midface) landmarks. We calculated the difference in the matching landmark coordinates from the two measurements (i.e., intra-observer error) and removed those that consistently exceeded an arbitrary difference of 7 voxels (0.125mm) between measurements (43). Furthermore, we used centroid sizes, the square root of the sum of squared Euclidean distances from each landmark to their own centroid, as a proxy for cranial and midface size (44).

Variations in skull shape were assessed using principal components analysis (PCA). Two types of PCA were carried out separately for the analysis of skull morphology: 1) a PCA based on variation in form (size and shape together) followed by; 2) PCA using the residuals of multivariate regression of Procrustes coordinates on centroid size to investigate the shape variation independent of size (shape only) (45,46). PCA of Procrustes coordinates is based on an eigenvalue decomposition of a covariance matrix, which transforms the Procrustes coordinates into scores along with principal components (PCs). In most cases, the first few PCs described most of the variance in the dataset. Each observation was scored for each principal axis and the score of an observation along the principal axes map in the morphospace was defined by the principal component axes using MorphoJ software (47).

4.3 Statistical analysis

For centroid sizes, the normal distribution of data was tested using the Kolmogorov-Smirnov non-parametric test. An independent t-test was employed to verify the existence of any significant differences in skull measurements between control and mutant groups.

4.4 Histology

The skulls of E14.5, 16.5, P0, and P7 mice were demineralized in 0.5 M EDTA for 1-7 days, dehydrated, embedded in paraffin wax in either frontal or sagittal orientations, and serially sectioned at 7 microns. Histological sections were stained with hematoxylin and eosin (H&E) following standard procedures. Bright-field images were taken using a DM5000B microscope with a DFC500 camera (Leica, Wetzlar, Germany).

5. Results

5.1 Notch signaling alters craniofacial morphology in *Jag1*[Ndr/Ndr] mice

Cranium including midface

3D GMA showed variations in the zygomatic process and the area where parietal, occipital, and squamosal bones intersect in mutant mice (Fig. 2). In addition, mutants had more convex crania from both frontal and lateral views and a longer snout. The first and second principal components (PC1 and PC2) in the Principal Component Analysis (PCA) accounted for 55.72% of the total variation, with PC1 comprising 30.85% and PC2 responsible for 24.87% of the total variation (Fig. 5a). PC1 of the Ndr mutants was more widely distributed along the horizontal axis compared to the PC2 vertical axis or PC1 of the control samples. The points representing the control samples were clustered into a limited region. This data revealed statistically significant differences between the two populations, with $p < 0.05$.

Right Mandible

3D GMA showed increased variation in the shape of the right mandible in Notch mutants, especially in the coronoid process area (Fig. 3). PC1 accounted for 44.56% of the total variation, whereas PC2 was responsible for 21.64. Thus, PC1 and PC2 were associated with 66.20% of the total variation (Fig. 5b). PC1 of the Ndr mutants were more widely distributed along the PC1 horizontal axis than the PC2 vertical axis. More variations in PC1 are shown in the wireframe of the right mandible. However, the data were not statistically significant ($p > 0.05$).

Left Mandible

3D GMA showed slightly less variations in the shape of the left mandible compared to the right in Notch mutants (Fig. 3). PC1 accounted for 33.50% of the total variation, whereas PC2 was responsible for 26.80%. PC1 and PC2 were associated with 60.30% of the total variation (Fig. 5c). The projected configuration positions were close to one another in this space, or even overlapped. This indicates that control and mutant left mandibles were similar in shape and not statistically significant ($p > 0.05$).

Both Mandibles

3D GMA indicated greater variation when both hemi-mandibles were analyzed together (Fig. 4). PC1 accounted for 48.04% of the total variation, whereas PC2 was responsible for 24.72%. PC1 and PC2 accounted for 72.76% of the total variation (Fig. 5d). This data showed that the average shape of both hemi-mandibles analyzed together in control and mutant mice was distinct. The morphological differences of control and mutant mandibles were statistically significant ($p < 0.05$).

5.2 The role of Notch signaling on tooth development using histological analysis

E14.5 Controls vs. Ndr mutants

Analyses of developing mandibular and maxillary first molars of control and Ndr mutant mice at E14.5 showed no differences at the cellular or tissue levels (Fig. 6). No differences were also noted in developing mandibular incisors of both control and Ndr mutant (Fig. 7). H&E staining from both samples showed clear and attached boundaries among each layer of tooth structures.

E16.5 Controls vs. Ndr mutants

Analyses of mandibular and maxillary incisors of control and Ndr mutant mice at E16.5 showed no differences at 10x and 20x magnification (Fig. 8).

P0 Controls vs. Ndr mutants

Analyses of mandibular and maxillary incisors and 1st molars of control and Ndr mutant mice at P0 showed no obvious differences (Fig. 9, 10). H&E staining of control and mutant teeth at 40x magnification show organized and attached boundaries among each layer of tooth structure. Ameloblast, stratum intermedium, enamel, and dentin layers are more clearly seen without any detachments among layers.

P7 Controls vs. Ndr mutants

P7 control and Ndr mutant teeth showed clear developmental differences. H&E staining of maxillary first and second molars of P7 control samples at 10x, 20x, and 40x magnifications all showed clear boundaries among different tooth layers with no zone of detachments (Fig. 10, 11). The maxillary and mandibular incisors of P7 wildtype samples also revealed similar clear outlines of different layers of the tooth structure with no zone of detachments (Fig. 10, 11).

H&E staining of maxillary first and second molars of P7 Ndr mutants showed clear zones of cell detachment between enamel and ameloblast layers in all 10x, 20x, and 40x magnifications. There was a clear white zone on the stained samples in this region of the tooth. There was also wax found between enamel and ameloblast layers supporting the

observation of ameloblast-enamel matrix detachment rather than histological artifact. Similar cell detachments between enamel and ameloblast layers were found in both maxillary and mandibular incisors of P7 Ndr samples. In addition, detachment between the ameloblast and stratum intermedium layers of the incisors were observed under 40x magnification.

5.3 The role of Notch signaling on tooth development using microCT analysis

MicroCT analysis of control and Ndr mutant dentition showed morphological differences in mandibular 1st molars (Fig. 12). We primarily focused on comparing the shape differences in controls versus Ndr mutants in adults and P7 samples based on our histological findings (Fig. 12). The microCT of adult and P7 teeth were generated to relate our 2D histological findings to the macrostructure data at a 3D level. The left mandibular molars in both adults and P7s were compared in order to consistently focus on one area of the teeth. In both adults and P7s, the cusp anatomy was not as clearly defined in Ndr mutants compared to controls. Particularly, the mesial marginal ridges of the first molars were significantly affected in mutants. The cusp tips also seemed to be significantly worn down in the adult molars.

6. Discussion

Early lethality at embryonic and peri-natal stages involved with inactivation of Notch signaling in knockout models has posed challenges in studying the role of Notch signaling during tooth and craniofacial development. In this study, the viability of *Jag1*[Ndr/Ndr] embryos recovered at E14.5, E16.5, P0, P7, and adults has allowed us to determine that Notch signaling regulates not only craniofacial morphology, but also specific areas and timing of developing teeth. We found that the *Jag1*[Ndr/Ndr] mouse with a Jag1 missense mutation showed abnormal craniofacial morphology and tooth development anomalies frequently seen in ALGS patients.

The 3D GMA findings in this study showed significant craniofacial morphological differences in *Jag1*[Ndr/Ndr] mutants compared to control. In the skull, notable discrepancies were found in the shape of zygomatic process, intersections between parietal, occipital, and squamosal bones, more convex cranium from both frontal and lateral views, and longer snout. In the mandible, the shape of the coronoid process was the only region of difference.

The microCT landmarks used for the 3D GMA suggest that the significant differences in the cranium relate to sutures in certain regions of the skull. In our mutant model, sutures between parietal and occipital bones, as well as intersection between parietal and squamosal bones appeared to be most affected. The anomalies in sutures may, in turn, influence surrounding structures, such as zygomatic processes and cranial shapes as a whole. These structural anomalies in mutant mice suggest correlations between 3D GMA findings in Ndr mutant mice and clinical observations documented in ALGS patients. There have been reports about a small population of human ALGS patients with craniosynostosis (9). Although Kamath et al. primarily discusses unilateral coronal craniosynostosis related

to ALGS, we can postulate from our findings that there may be multiple sutures that are affected by ALGS. It has been known that premature fusion of cranial sutures on a larger scale leads to abnormal skull shape, as seen in other diseases associated with craniosynostosis, such as Crouzon and Pfeiffer syndromes (48). It can also lead to deformities in surrounding structures, such as eyes, nose, and ears. Similar craniofacial dysmorphisms associated with ALGS have been previously documented involving not only craniosynostosis, but also a prominent forehead, moderate hypertelorism with deep-set eyes, a saddle or straight nose with a flattened, bulbous tip, and large ears (9,49). Our 3D GMA findings suggested that the $Jag1^{Ndr/Ndr}$ mutants in our study showed a longer snout length, which was contrary to what other studies found in the similar $Jag1^{Ndr/Ndr}$ models. Both Andersson et al. and Humphreys et al. found reduced snout lengths (25,50). Nevertheless, our study shows that the phenotypic variations captured in the Ndr mutant mice may closely correlate to the clinical phenotype previously observed in human ALGS.

We identified histological changes in the ameloblast-enamel matrix and ameloblast-SI interfaces in Ndr mutants between P0 and P7. This is the first documented report demonstrating specific developmental defects and the stages at which these defects were initially observed histologically due to mutations in Notch signaling. Histological sections of the incisors and the molars showed no differences between control and Ndr mutants at E14.5, E16.5, and P0. There were no gross dysmorphisms in the overall tooth shape or changes in tooth development. In P7 incisors and molars, however, we found that there was a distinct separation between enamel matrix and ameloblasts. The presence of wax between the enamel matrix and ameloblasts further confirmed the physical separation between the two layers. The incisors also showed a fine line of disconnection between the

ameloblasts and the SI layer. Jheon et al. reported similar detachment patterns in the ameloblast-SI interface of the incisors when the inhibitory antibodies against principal components of the Notch signaling pathway, such as Notch1, Notch2, Jag1, and Jag2 were injected into adult mice (32). The same detached layers in our Ndr mutant incisors and the Notch antibody study reveals that the role of normal Notch signaling is critical in ameloblast-SI adhesion. One further explanation about the loss of adhesion is the defect in normal desmosome function. These transmembrane proteins that usually provide strong cell-cell adhesion can lead to changes in enamel formation when abnormalities are introduced during amelogenesis. Two main genes, *Perp* and *Pvrl1*, are associated with desmosomes in enamel formation (30). Any mutations in these genes are known to cause disintegration of cell-cell attachments. It has been previously documented that Notch signaling regulates the major desmosome family called cadherin (51). There also has been evidence that Notch signaling controls desmosome-specific factors, such as Perp, in mouse tooth incisors (32).

The role of Notch signaling in early cell fate determination during development may explain detachment between ameloblasts and the enamel matrix. An *in vitro* study with the *Drosophila Notch* gene has also reported comparable findings that not only were the Notch genes expressed in SI-like cells, but were also involved in tooth morphogenesis and early determination of ameloblasts (29). The process of normal tooth development involves tightly regulated protein expressions, such as growth factors, transcription factors, and progressive interactions between epithelial and mesenchymal cells. Notch signaling mutations, however, may change the fate of epithelial and mesenchymal cells. The loss of normal interaction between ameloblasts and the enamel matrix may potentially be

explained by the abnormal cell fate determination and differentiation of ameloblasts leading to defective, lessened, or absent ability to generate normal enamel matrix property (29).

Notch signaling mutations may also cause an overall disintegration of developing ameloblasts and their neighboring layers because of defects in amelogenin. Ameloblasts secrete amelogenins, which are highly conserved proteins that regulate dental enamel thickness and structure in humans and mice (52–54). Amelogenins are secreted before teeth erupt into the oral cavity, and any abnormal secretion leads to changes in highly organized and mineralized enamel layer (55,56). Amelogenin knockout mice showed that ameloblast attachment to the developing enamel surface was weakened (53). Another study showed that ameloblasts express low levels of endogenous amelogenin during fetal development and birth (11). Furthermore, there is evidence that SI cells may also express low levels of amelogenin (57–59). The adult molars in our microCT images showed significantly worn-down cusps. Even though the P7 molars only started to reveal cusp morphology differences, the considerable amount of attrition on the adult molars suggests that the weakened tooth structure due to abnormal enamel development may have led to attrition in adult molars over time. The finding that changes in Notch signaling pathway are associated with defects in amelogenin may be another potential reason for the developmental dental defects that we discovered.

Even though genetic mutations causing ALGS have been studied extensively, ALGS is considered a highly variable, multi-organ disease with no clear genotype-phenotype correlations. There is ample evidence to prove that ALGS is caused by heterozygous mutations in the fundamental components of the Notch signaling pathway, namely Jag1 and

Notch2, and that haploinsufficiency with deletions in a single Jag1 allele is sufficient to cause the disease (25,60). However, many genotype-phenotype correlation studies have not been able to establish a strong connection between mutation type and clinical manifestation or severity (22,61). Our 3D GMA study also showed that the data points for the Ndr mutants were widely scattered along the PCA axes compared to control data points. Both our mouse study and the human clinical studies suggest high variability in the expression of altered Notch signaling pathways, possibly due to differential penetrance of the genetic mutations. Interestingly, patients with the same mutations, including the ones from the same family, showed clinical variability in disease phenotypes. The variable expressivity of the disease with differential penetrance makes it challenging to identify this link.

Because some ALGS patients may present with more severe systemic manifestations that can be life-threatening, associated craniofacial and dental effects may be of less concern. However, dysmorphic facial features are considered one of the best diagnostic characteristics of ALGS even though chronic cholestasis is the most common presenting trait (62). Our study demonstrated specific changes in craniofacial morphology and identified developmental defects in mouse molars at P7. It will be helpful in the future to evaluate the detailed differences in ameloblasts and their surrounding cells through transmission electron microscopy (TEM), tooth mineralization differences using scanning electron microscopy (SEM), explore variable expressivity of principal Notch signaling genes through immunofluorescence staining, and use similar 3D GMA methods to documents tooth morphology. Ultimately, these data can be gathered and analyzed to correlate genotypes and phenotypes of ALGS in craniofacial and dental development.

In summary, analyses of *Jag1*[Ndr/Ndr] mice underscored the importance of Notch signaling in craniofacial shape and dental development. Specifically, disruption in Notch signaling led to: 1) specific changes in craniofacial morphology; 2) defective enamel formation and disfigured cusp shapes due to, in part, defects in cell-cell (ameloblast-SI) and cell-matrix (ameloblast-enamel matrix) adhesion; 3) potentially weakened tooth structures due to abnormal tooth development and mineralization that occurred between P0 to P7 stages. Thus, our study confirmed the importance of Notch signaling in Alagille syndrome, as well as in proper craniofacial and dental development.

7. References

1. Alagille D, Odièvre M, Gautier M, Dommergues JP. Hepatic ductular hypoplasia associated with characteristic facies, vertebral malformations, retarded physical, mental, and sexual development, and cardiac murmur. J Pediatr. 1975 Jan;86(1):63–71.

2. Emerick KM, Rand EB, Goldmuntz E, Krantz ID, Spinner NB, Piccoli DA. Features of Alagille syndrome in 92 patients: frequency and relation to prognosis. Hepatology. 1999 Mar;29(3):822–9.

3. Berniczei-Royko A, Chałas R, Mitura I, Nagy K, Prussak E. Medical and dental management of Alagille syndrome: a review. Med Sci Monit. 2014 Mar 24;20:476–80.

4. McDaniell R, Warthen DM, Sanchez-Lara PA, Pai A, Krantz ID, Piccoli DA, et al. NOTCH2 mutations cause Alagille syndrome, a heterogeneous disorder of the notch signaling pathway. Am J Hum Genet. 2006 Jul;79(1):169–73.

5. Spinner NB. Alagille syndrome and the notch signaling pathway: New insights into human development. Gastroenterology. 1999 May;116(5):1257–60.

6. Rosenfield NS, Kelley MJ, Jensen PS, Cotlier E, Rosenfield AT, Riely CA. Arteriohepatic dysplasia: radiologic features of a new syndrome. AJR Am J Roentgenol. 1980 Dec;135(6):1217–23.

7. Zanotti S, Canalis E. Notch and the skeleton. Mol Cell Biol. 2010 Feb;30(4):886–96.

8. Alagille D, Odièvre M, Gautier M, Dommergues JP. Facies in alagille syndrome. J Pediatr. 1984 Mar;104(3):487.

9. Kamath BM, Stolle C, Bason L, Colliton RP, Piccoli DA, Spinner NB, et al. Craniosynostosis in Alagille syndrome. Am J Med Genet. 2002 Oct 1;112(2):176–80.

10. Faux CH, Turnley AM, Epa R, Cappai R, Bartlett PF. Interactions between fibroblast growth factors and Notch regulate neuronal differentiation. J Neurosci. 2001 Aug 1;21(15):5587–96.

11. Harada H, Kettunen P, Jung HS, Mustonen T, Wang YA, Thesleff I. Localization of putative stem cells in dental epithelium and their association with Notch and FGF signaling. J Cell Biol. 1999 Oct 4;147(1):105–20.

12. Ho NC, Lacbawan F, Francomano CA, Ho V. Severe hypodontia and oral xanthomas in Alagille syndrome. Am J Med Genet. 2000 Jul 31;93(3):250–2.

13. Amaral THA do, Guerra C de S, Bombonato-Prado KF, Garcia de Paula E Silva FW, de Queiroz AM. Tooth pigmentation caused by bilirubin: a case report and histological evaluation. Spec Care Dentist. 2008 Dec;28(6):254–7.

14. Olczak-Kowalczyk D, Kowalczyk W, Krasuska-Sławińska E, Dądalski M, Kostewicz K, Pawłowska J. Oral health and liver function in children and adolescents with cirrhosis of the liver. Prz Gastroenterol. 2014 Mar 1;9(1):24–31.

15. Guimarães LP, Silva TA. Green teeth associated with cholestasis caused by sepsis: a case report and review of the literature. Oral Surg Oral Med Oral Pathol Oral Radiol Endod. 2003 Apr;95(4):446–51.

16. Al-Mutawa S, Mathews B, Salako N. Oral findings in Alagille syndrome. A case report. Med Princ Pract. 2002 Sep;11(3):161–3.

17.   Chatterjee M, Mason C. Talon cusps presenting in a child with Alagille's syndrome--a case report. J Clin Pediatr Dent. 2007;32(1):61–3.

18.   Cozzani M, Fontana M. Macrodontic maxillary incisor in alagille syndrome. Dent Res J (Isfahan). 2012 Dec;9(Suppl 2):S251-4.

19.   Farronato M. Oro-Facial Findings in Orthodontic Alagille Patient: First Documented Case Presenting Multiple Agenesis. MRD. 2018 Jan 23;1(4).

20.   Turnpenny PD, Ellard S. Alagille syndrome: pathogenesis, diagnosis and management. Eur J Hum Genet. 2012 Mar;20(3):251–7.

21.   Crosnier C, Driancourt C, Raynaud N, Dhorne-Pollet S, Pollet N, Bernard O, et al. Mutations in JAGGED1 gene are predominantly sporadic in Alagille syndrome. Gastroenterology. 1999 May;116(5):1141–8.

22.   Warthen DM, Moore EC, Kamath BM, Morrissette JJD, Sanchez-Lara PA, Piccoli DA, et al. Jagged1 (JAG1) mutations in Alagille syndrome: increasing the mutation detection rate. Hum Mutat. 2006 May;27(5):436–43.

23.   Xue Y, Gao X, Lindsell CE, Norton CR, Chang B, Hicks C, et al. Embryonic lethality and vascular defects in mice lacking the Notch ligand Jagged1. Hum Mol Genet. 1999 May;8(5):723–30.

24.   McCright B, Lozier J, Gridley T. A mouse model of Alagille syndrome: Notch2 as a genetic modifier of Jag1 haploinsufficiency. Development. 2002 Feb;129(4):1075–82.

25.   Andersson ER, Chivukula IV, Hankeova S, Sjöqvist M, Tsoi YL, Ramsköld D, et al. Mouse model of alagille syndrome and mechanisms of jagged1 missense mutations.

Gastroenterology. 2018;154(4):1080–95.

26. Kamath BM, Bauer RC, Loomes KM, Chao G, Gerfen J, Hutchinson A, et al. NOTCH2 mutations in Alagille syndrome. J Med Genet. 2012 Feb;49(2):138–44.

27. Gilbert MA, Bauer RC, Rajagopalan R, Grochowski CM, Chao G, McEldrew D, et al. Alagille syndrome mutation update: Comprehensive overview of JAG1 and NOTCH2 mutation frequencies and insight into missense variant classification. Hum Mutat. 2019 Aug 26;40(12):2197–220.

28. Jheon AH, Seidel K, Biehs B, Klein OD. From molecules to mastication: the development and evolution of teeth. Wiley Interdiscip Rev Dev Biol. 2013 Apr;2(2):165–82.

29. Mitsiadis TA, Lardelli M, Lendahl U, Thesleff I. Expression of Notch 1, 2 and 3 is regulated by epithelial-mesenchymal interactions and retinoic acid in the developing mouse tooth and associated with determination of ameloblast cell fate. J Cell Biol. 1995 Jul;130(2):407–18.

30. Jheon AH, Mostowfi P, Snead ML, Ihrie RA, Sone E, Pramparo T, et al. PERP regulates enamel formation via effects on cell-cell adhesion and gene expression. J Cell Sci. 2011 Mar 1;124(Pt 5):745–54.

31. Sasaki T, Segawa K, Takiguchi R, Higashi S. Intercellular junctions in the cells of the human enamel organ as revealed by freeze-fracture. Arch Oral Biol. 1984;29(4):275–86.

32. Jheon AH, Prochazkova M, Meng B, Wen T, Lim Y-J, Naveau A, et al. Inhibition of notch signaling during mouse incisor renewal leads to enamel defects. J Bone Miner Res.

2016 Jan;31(1):152–62.

33. Hori K, Sen A, Artavanis-Tsakonas S. Notch signaling at a glance. J Cell Sci. 2013 May 15;126(Pt 10):2135–40.

34. Pakvasa M, Haravu P, Boachie-Mensah M, Jones A, Coalson E, Liao J, et al. Notch signaling: Its essential roles in bone and craniofacial development. Genes Dis. 2021 Jan;8(1):8–24.

35. Dong Y, Jesse AM, Kohn A, Gunnell LM, Honjo T, Zuscik MJ, et al. RBPjkappa-dependent Notch signaling regulates mesenchymal progenitor cell proliferation and differentiation during skeletal development. Development. 2010 May;137(9):1461–71.

36. Rutkovskiy A, Stensløkken K-O, Vaage IJ. Osteoblast differentiation at a glance. Med Sci Monit Basic Res. 2016 Sep 26;22:95–106.

37. Bouvier M, Hylander WL. The effect of dietary consistency on morphology of the mandibular condylar cartilage in young macaques (Macaca mulatta). Prog Clin Biol Res. 1982;101:569–79.

38. Sylvester AD. A geometric morphometric analysis of the medial tibial condyle of African hominids. Anat Rec (Hoboken). 2013 Oct;296(10):1518–25.

39. Freudenthaler J, Čelar A, Ritt C, Mitteröcker P. Geometric morphometrics of different malocclusions in lateral skull radiographs. J Orofac Orthop. 2017 Jan;78(1):11–20.

40. Hassan MG, Kaler H, Zhang B, Cox TC, Young N, Jheon AH. Effects of Multi-Generational Soft Diet Consumption on Mouse Craniofacial Morphology. Front

Physiol. 2020 Jul 10;11:783.

41.   Mitteroecker P, Gunz P, Bernhard M, Schaefer K, Bookstein FL. Comparison of cranial ontogenetic trajectories among great apes and humans. J Hum Evol. 2004 Jun;46(6):679–97.

42.   Wiley DF, Amenta N, Alcantara D, Ghosh D, Kil Y, Delson E, et al. Evolutionary Morphing (In Proceedings). Minneapolis, Minnesota: Proceedings of IEEE Visualization 2005; 2005.

43.   Maga AM, Navarro N, Cunningham ML, Cox TC. Quantitative trait loci affecting the 3D skull shape and size in mouse and prioritization of candidate genes in-silico. Front Physiol. 2015 Mar 26;6:92.

44.   Dryden IL, Mardia KV. Statistical Shape Analysis. 1st ed. Chichester: Wiley; 1998.

45.   Falsetti AB, Jungers WL, Colle TM. Morphometrics of the callitrichid forelimb: A case study in size and shape. Int J Primatol. 1993 Aug;14(4):551–72.

46.   Darroch JN, Mosimann JE. Canonical and principal components of shape. Biometrika. 1985 Jan 1;72(2):241–52.

47.   Klingenberg CP. MorphoJ: an integrated software package for geometric morphometrics. Mol Ecol Resour. 2011 Mar;11(2):353–7.

48.   Johnson D, Wilkie AOM. Craniosynostosis. Eur J Hum Genet. 2011 Apr;19(4):369–76.

49.   Kamath BM, Loomes KM, Oakey RJ, Emerick KEM, Conversano T, Spinner NB, et al. Facial features in Alagille syndrome: specific or cholestasis facies? Am J Med Genet. 2002 Oct 1;112(2):163–70.

50. Humphreys R, Zheng W, Prince LS, Qu X, Brown C, Loomes K, et al. Cranial neural crest ablation of Jagged1 recapitulates the craniofacial phenotype of Alagille syndrome patients. Hum Mol Genet. 2012 Mar 15;21(6):1374–83.

51. Bazzi H, Demehri S, Potter CS, Barber AG, Awgulewitsch A, Kopan R, et al. Desmoglein 4 is regulated by transcription factors implicated in hair shaft differentiation. Differentiation. 2009 Dec;78(5):292–300.

52. Couwenhoven RI, Snead ML. Early determination and permissive expression of amelogenin transcription during mouse mandibular first molar development. Dev Biol. 1994 Jul;164(1):290–9.

53. Chen X, Li Y, Alawi F, Bouchard JR, Kulkarni AB, Gibson CW. An amelogenin mutation leads to disruption of the odontogenic apparatus and aberrant expression of Notch1. J Oral Pathol Med. 2011 Mar;40(3):235–42.

54. Robinson C, Kirkham J, Brookes SJ, Bonass WA, Shore RC. The chemistry of enamel development. Int J Dev Biol. 1995 Feb;39(1):145–52.

55. Smith CE. Cellular and chemical events during enamel maturation. Crit Rev Oral Biol Med. 1998;9(2):128–61.

56. Margolis HC, Beniash E, Fowler CE. Role of macromolecular assembly of enamel matrix proteins in enamel formation. J Dent Res. 2006 Sep;85(9):775–93.

57. Tompkins K, Alvares K, George A, Veis A. Two related low molecular mass polypeptide isoforms of amelogenin have distinct activities in mouse tooth germ differentiation in vitro. J Bone Miner Res. 2005 Feb;20(2):341–9.

58. Chen E, Piddington R, Decker S, Park J, Yuan ZA, Abrams WR, et al. Regulation of amelogenin gene expression during tooth development. Dev Dyn. 1994 Mar;199(3):189–98.

59. Iacob S, Veis A. Identification of temporal and spatial expression patterns of amelogenin isoforms during mouse molar development. Eur J Oral Sci. 2006 May;114 Suppl 1:194–200; discussion 201.

60. Fischetto R, Palmieri VV, Tripaldi ME, Gaeta A, Michelucci A, Delvecchio M, et al. Alagille syndrome: A novel mutation in JAG1 gene. Front Pediatr. 2019 May 15;7.

61. Kamath BM, Baker A, Houwen R, Todorova L, Kerkar N. Systematic review: the epidemiology, natural history, and burden of alagille syndrome. J Pediatr Gastroenterol Nutr. 2018;67(2):148–56.

62. Jesina D. Alagille syndrome: an overview. Neonatal Netw. 2017 Nov 1;36(6):343–7.

Figures
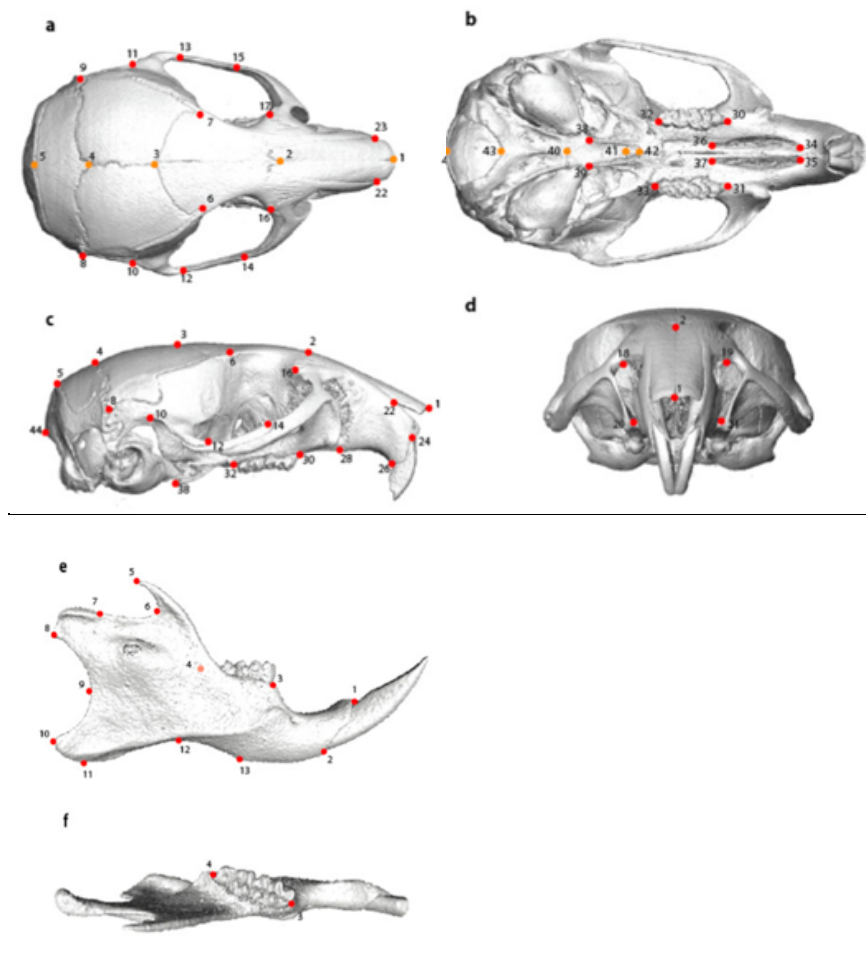
Figure 1. (a) Landmarks on the skull, dorsal view; (b) Landmarks on the skull, ventral view; (c) Landmarks on the skull, right lateral view; (d) Landmarks on the skull, frontal view; (e) Landmarks on the right mandible, lateral view; (f) Landmarks on the right mandible, dorsal view (Descriptions of landmarks to follow the figures)
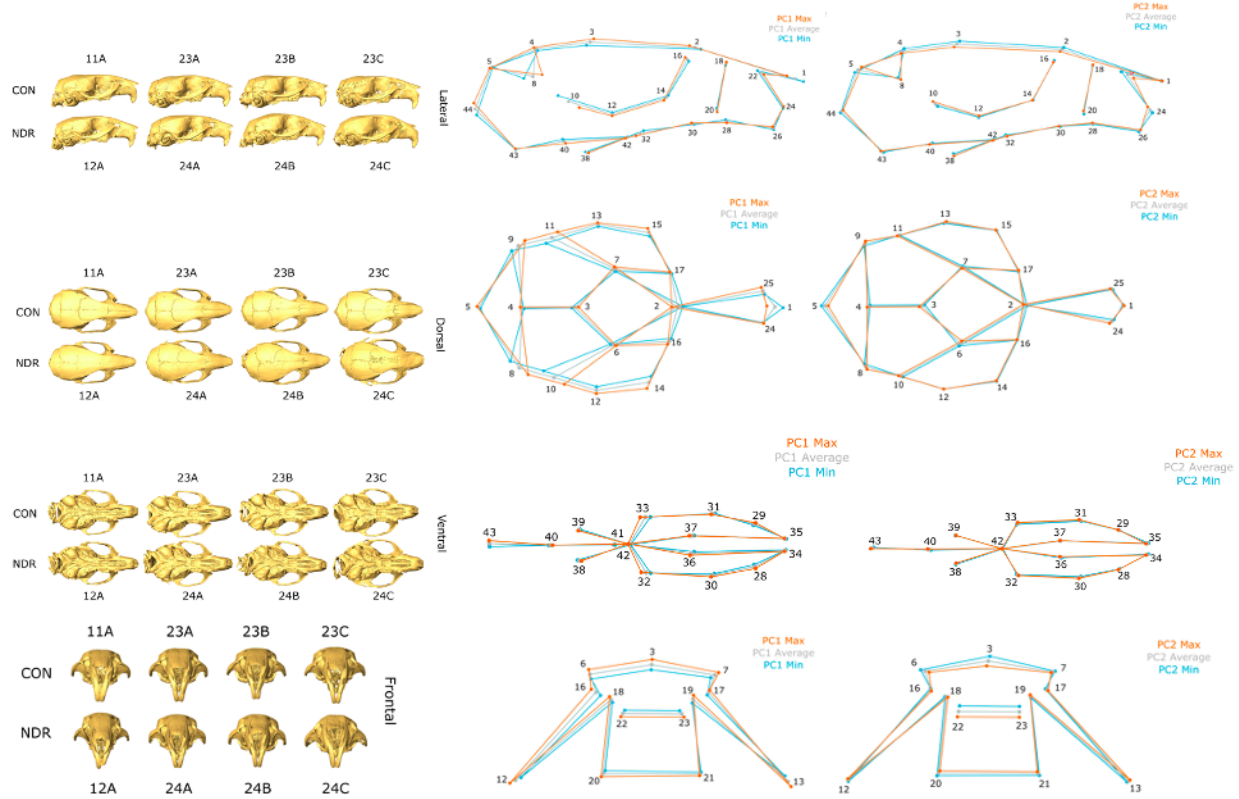
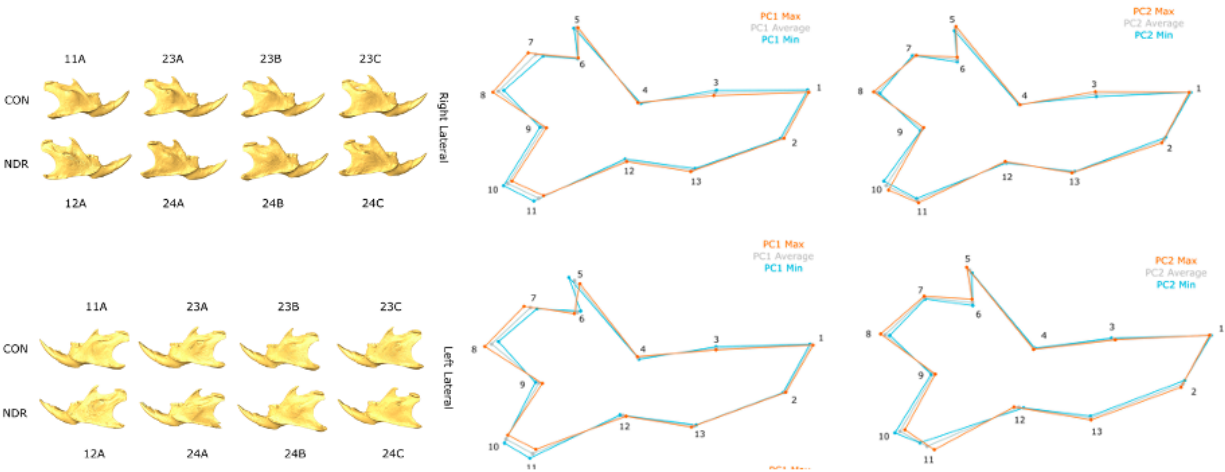**Figure 2.** 3D GMA of the skull in lateral, dorsal, ventral, and frontal views with the corresponding 2D wireframes

Figure 3. 3D GMA of the separate right and left mandibles in lateral view with the corresponding 2D wireframes
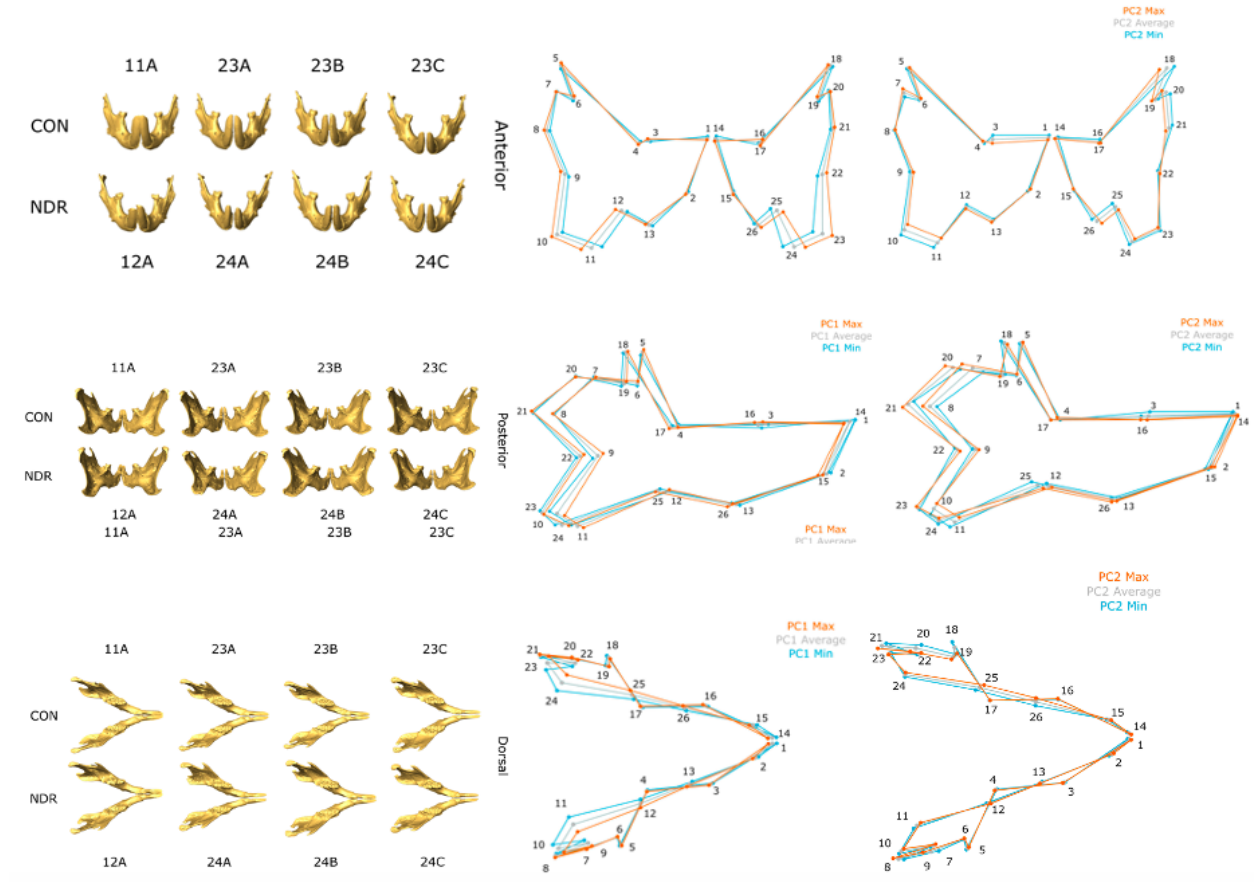
Figure 4. 3D GMA of the combined right and left mandibles in lateral view with the corresponding 2D wireframes
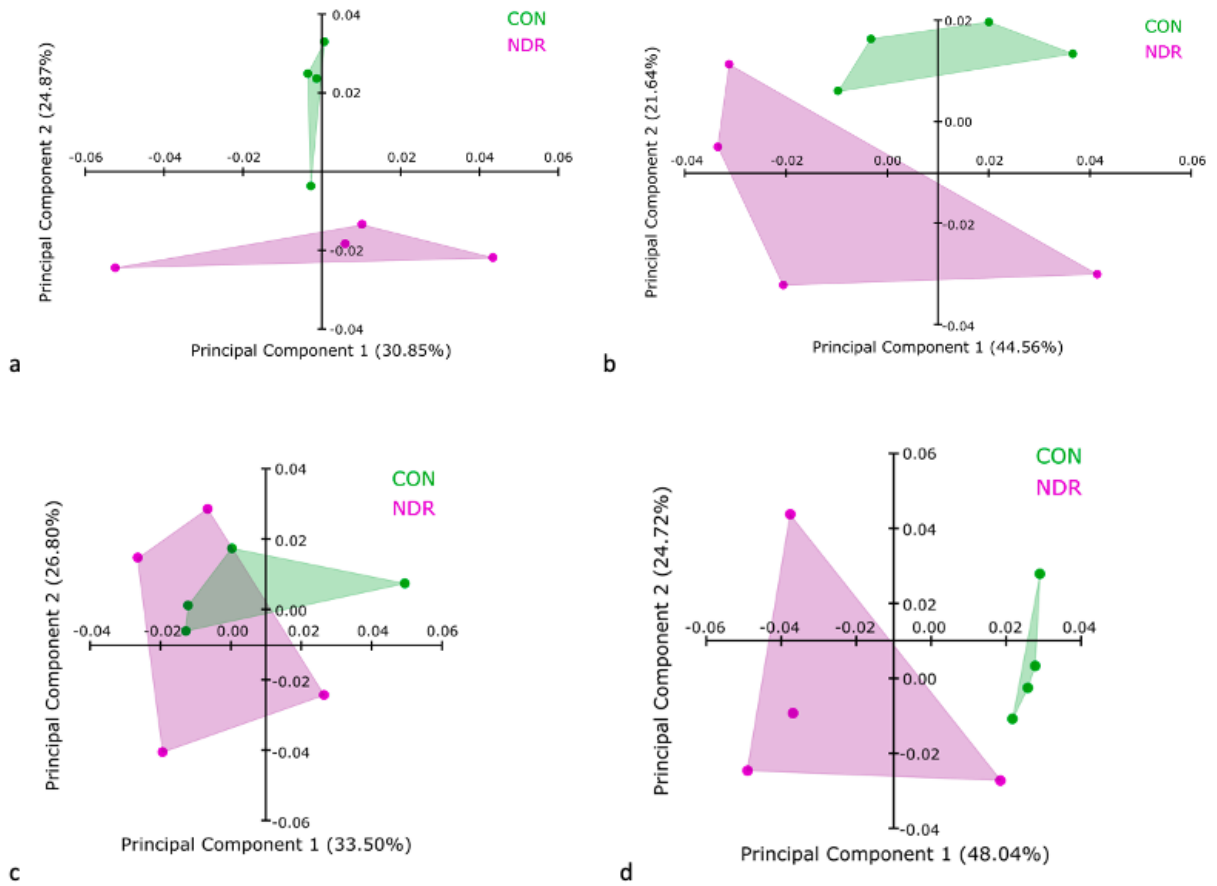
Figure 5. (a) PCA of the skull; (b) PCA of the right mandible; (c) PCA of the left mandible; (d) PCA of the combined mandibles
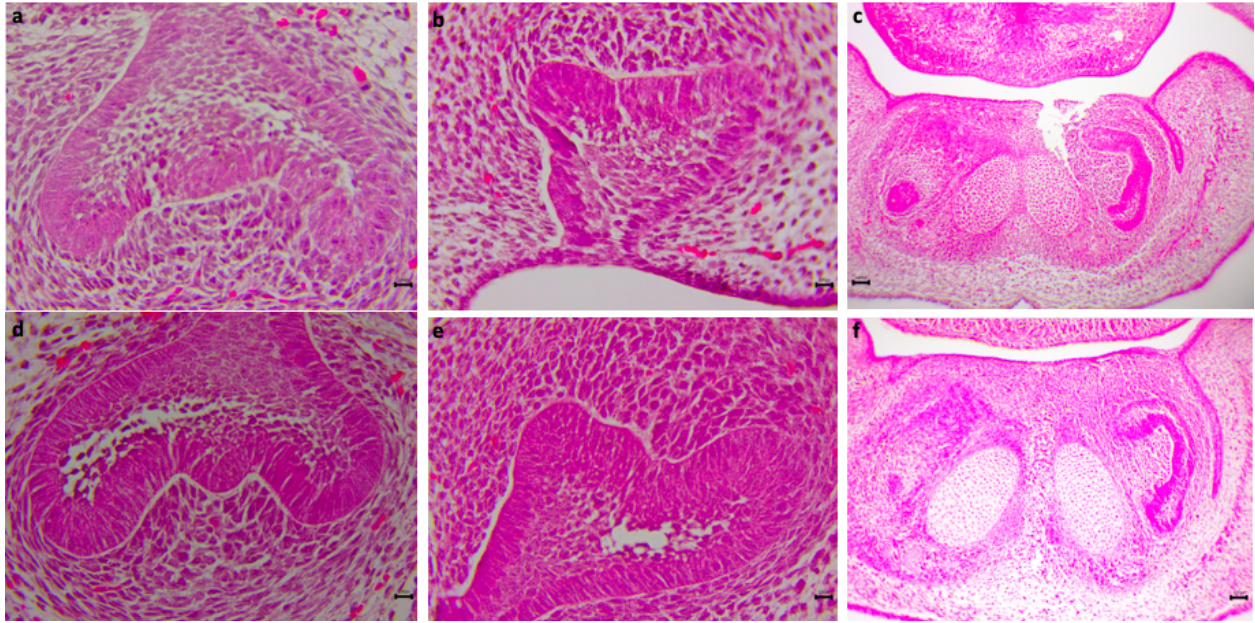
Figure 6. Frontal sections of (a) E14.5 control mandibular molar; (b) E14.5 control maxillary molar; (c) E14.5 control mandibular incisors; (d) E14.5 mutant mandibular molar; (e) E14.5 mutant maxillary molar; (f) E14.5 mutant mandibular incisors
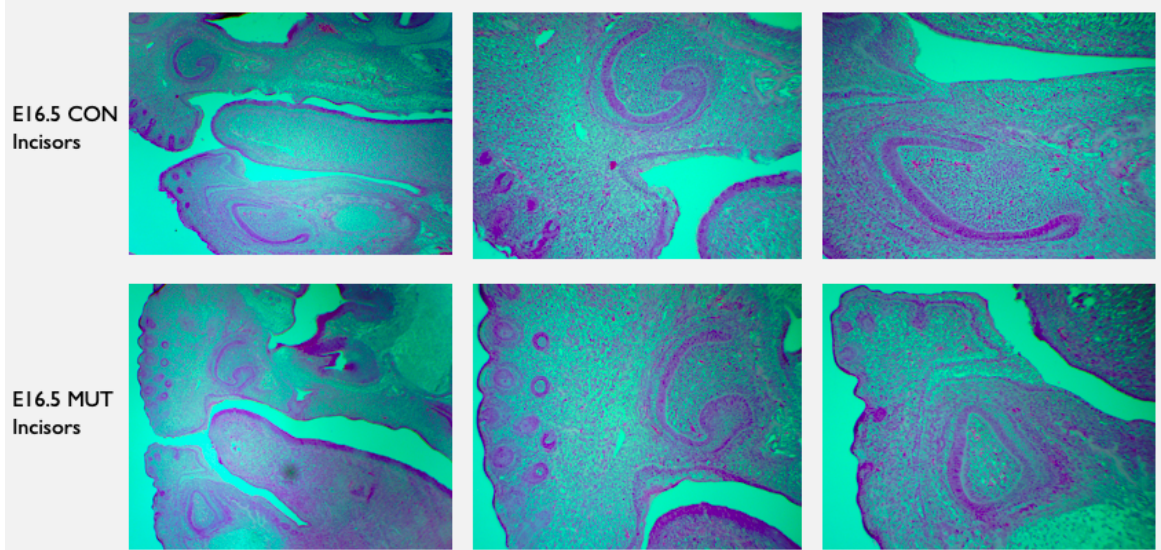

Figure 7. Sagittal sections of maxillary and mandibular incisors of controls (top row) versus mutants (bottom row) at E16.5
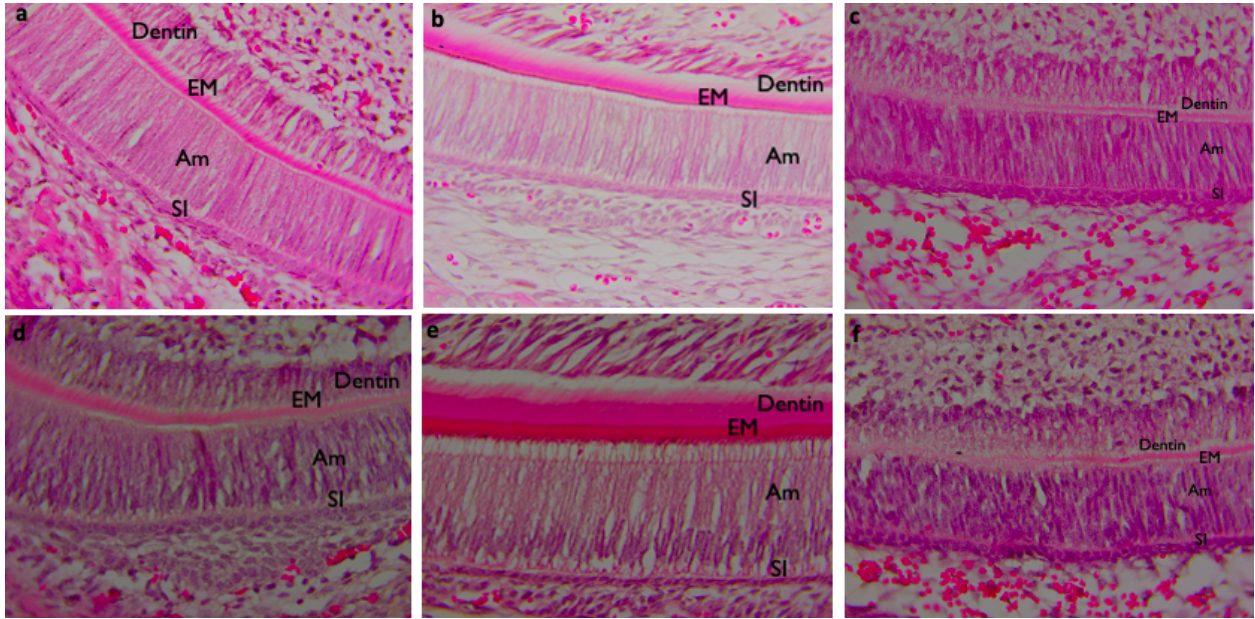
Figure 8. 40x magnification view of (a) P0 control maxillary incisors; (b) P0 control mandibular incisors; (c) P0 control maxillary first molar; (d) P0 mutant maxillary incisors; (e) P0 mutant mandibular incisors; (f) P0 mutant maxillary first molar
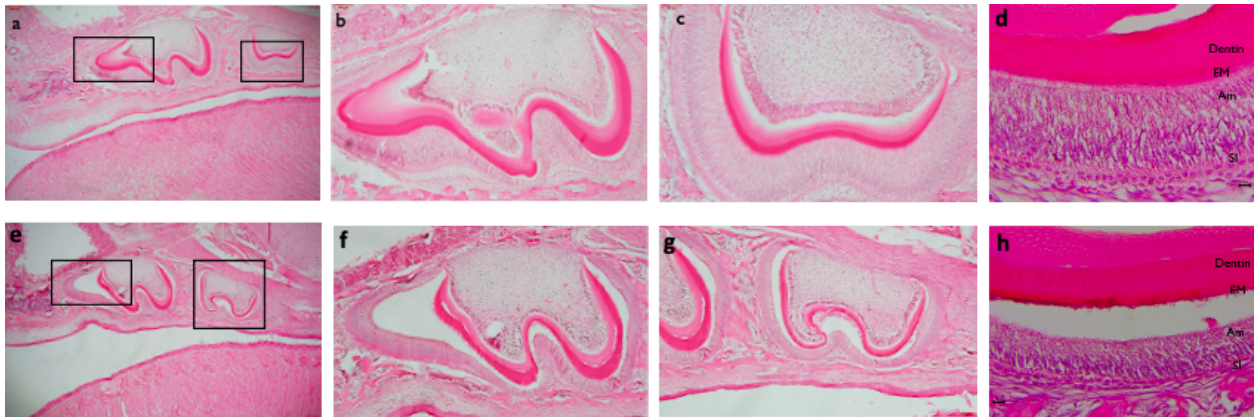

Figure 9. Sagittal view of (a) P7 control maxillary first and second molars in 10x; (b) P7 control maxillary first molar in 20x; (c) P7 control maxillary second molar in 20x; (d) P7 control molar in 40x; (e) P7 mutant maxillary first and second molars in 10x; (f) P7 mutant maxillary first molar in 20x; (g) P7 mutant maxillary second molar in 20x; (h) P7 mutant molar in 40x
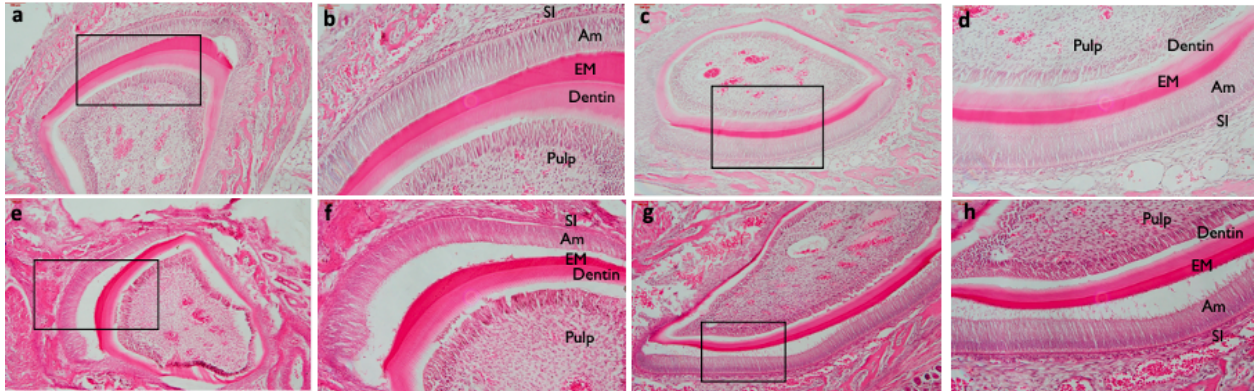
Figure 10. (a) P7 control maxillary incisor in 10x; (b) P7 control maxillary incisor in 20x; (c) P7 control mandibular incisor in 10x; (d) P7 control mandibular incisor in 20x; (e) P7 mutant maxillary incisor in 10x; (f) P7 mutant maxillary incisor in 20x; (g) P7 mutant mandibular incisor in 10x; (h) P7 mutant mandibular incisor in 20x
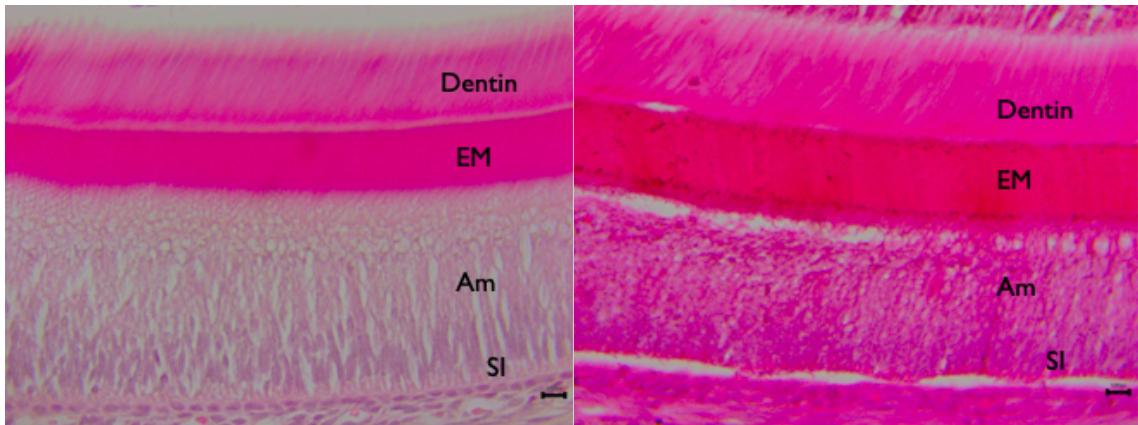

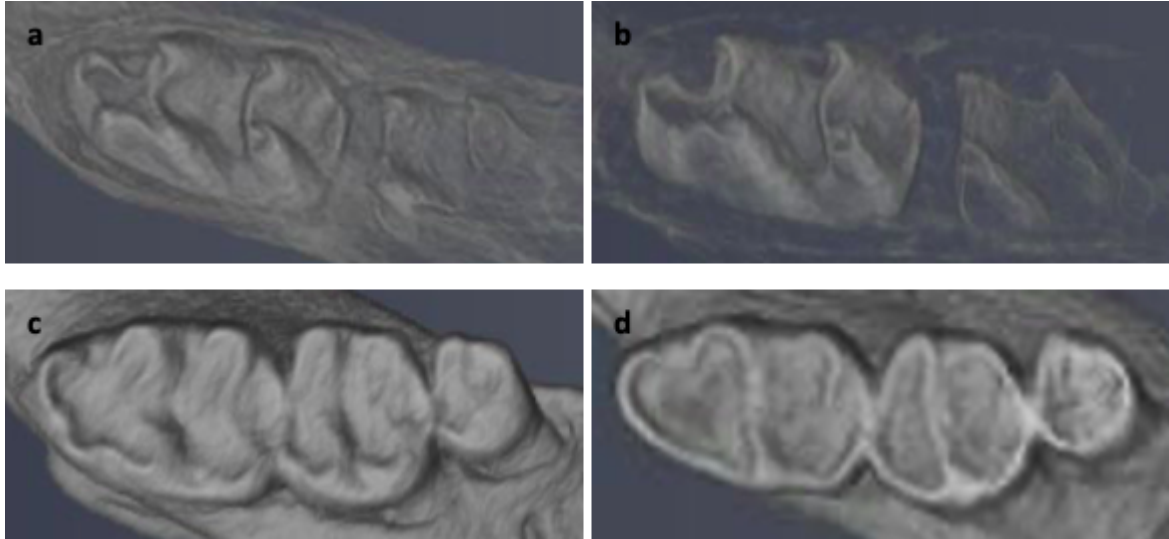**Figure 11.** P7 control incisor in 40x (left); P7 mutant incisor in 40x (right)

Figure 12. MicroCT images of (a) P7 control mandibular molars; (b) P7 mutant mandibular molars; (c) Adult control mandibular molars; (d) Adult mutant mandibular molars

Tables

Table 1. Descriptions of the skull landmarks

Point #s	Location
1	Nasal bone's most anterior suture
2	Nasal bone's most posterior suture
3	Frontal bone's most posterior suture
4	Parietal bone's most posterior suture
5	Interparietal bone's most posterior point on the median line
6	Right side, frontal-squamosal intersection at temporal crest
7	Left side, frontal-squamosal intersection at temporal crest
8	Right side, intersection between parietal, occipital and squamosal bones
9	Left side, intersection between parietal, occipital and squamosal bones
10	Right, most posterior junction of squamosal bone and the zygomatic process of the squamosal bone
11	Left, most posterior junction of squamosal bone and the zygomatic process of the squamosal bone
12	Right side, most anterior suture of jugal bone and the zygomatic process of the maxillary bone
13	Left side, most anterior suture of jugal bone and the zygomatic process of the maxillary bone
14	Right side, mid zygomatic bone
15	Left side, mid zygomatic bone
16	Right side, intersection of frontal process of maxilla with frontal and lacrimal bones
17	Left side, intersection of frontal process of maxilla with frontal and lacrimal bones
18	Right side, midpoint of the anterior zygomatic process (frontal view)
19	Left side, midpoint of the anterior zygomatic process (frontal view)
20	Most superior and lateral point of the right incisor alveolus
21	Most superior and lateral point of the left incisor alveolus
22	Right side, most anterior point at intersection of premaxillae and nasal bones
23	Left side, most anterior point at intersection of premaxillae and nasal bones
24	Right side, most superior point of the incisor alveolus
25	Left side, most superior point of the incisor alveolus (not shown)
26	Right side, most inferior anterior point of the incisor alveolus
27	Left side, most inferior anterior point of the incisor alveolus (not shown)
28	Right side, most inferior point of the zygomatic process
29	Left side, most inferior point of the zygomatic process (not shown)
30	Right side, most anterior point of the first molar alveolus
31	Left side, most anterior point of the first molar alveolus
32	Right side, most posterior point of the third molar alveolus
33	Left side, most posterior point of the third molar alveolus
34	Right side, most anterior point of the anterior palatine foramen
35	Left side, most anterior point of the anterior palatine foramen
36	Right side, most posterior point of the anterior palatine foramen
37	Left side, most posterior point of the anterior palatine foramen

Table 2. Descriptions of the mandible landmarks

Point #s	Location
1	Most superior point of the incisor alveolus
2	Most inferior point of the incisor alveolus
3	Most anterior point of the first molar alveolus
4	Most posterior point of the third molar alveolus
5	Most posterior tip of the coronoid process
6	Most anterior/inferior concave point of the coronoid process
7	Most anterior point of the articulare surface of the coronoid process
8	Most posterior tip of the condyle
9	Most anterior concave point between the condyle and angle of the mandible
10	Most posterior tip of the mandibular angle
11	Most inferior point of the mandibular angle
12	Ascending ramus dorsal-most ventral point
13	Most inferior point of alveolar region

Publishing Agreement

It is the policy of the University to encourage open access and broad distribution of all theses, dissertations, and manuscripts. The Graduate Division will facilitate the distribution of UCSF theses, dissertations, and manuscripts to the UCSF Library for open access and distribution. UCSF will make such theses, dissertations, and manuscripts accessible to the public and will take reasonable steps to preserve these works in perpetuity.

I hereby grant the non-exclusive, perpetual right to The Regents of the University of California to reproduce, publicly display, distribute, preserve, and publish copies of my thesis, dissertation, or manuscript in any form or media, now existing or later derived, including access online for teaching, research, and public service purposes.

Ji Hyun Taluk _____   6/6/2021_____
               Author Signature   Date